AMERICAN SOCIETY FOR MICROBIOLOGY | Journal of Bacteriology®

RESEARCH ARTICLE

Effects of Increasing the Affinity of CarD for RNA Polymerase on *Mycobacterium tuberculosis* Growth, rRNA Transcription, and Virulence

Ashley L. Garner,[a] Jayan Rammohan,[b] Jeremy P. Huynh,[a] Lucas M. Onder,[c] James Chen,[d] Brian Bae,[d] Drake Jensen,[b] Leslie A. Weiss,[a] Ana Ruiz Manzano,[b] Seth A. Darst,[d] Elizabeth A. Campbell,[d] Bryce E. Nickels,[c] Eric A. Galburt,[b] Christina L. Stallings[a]

Department of Molecular Microbiology, Washington University School of Medicine, St. Louis, Missouri, USA[a]; Department of Biochemistry and Molecular Biophysics, Washington University School of Medicine, St. Louis, Missouri, USA[b]; Department of Genetics and Waksman Institute of Microbiology, Rutgers University, Piscataway, New Jersey, USA[c]; Laboratory of Molecular Biophysics, The Rockefeller University, New York, New York, USA[d]

ABSTRACT CarD is an essential RNA polymerase (RNAP) interacting protein in *Mycobacterium tuberculosis* that stimulates formation of RNAP-promoter open complexes. CarD plays a complex role in *M. tuberculosis* growth and virulence that is not fully understood. Therefore, to gain further insight into the role of CarD in *M. tuberculosis* growth and virulence, we determined the effect of increasing the affinity of CarD for RNAP. Using site-directed mutagenesis guided by crystal structures of CarD bound to RNAP, we identified amino acid substitutions that increase the affinity of CarD for RNAP. Using these substitutions, we show that increasing the affinity of CarD for RNAP increases the stability of the CarD protein in *M. tuberculosis*. In addition, we show that increasing the affinity of CarD for RNAP increases the growth rate in *M. tuberculosis* without affecting 16S rRNA levels. We further show that increasing the affinity of CarD for RNAP reduces *M. tuberculosis* virulence in a mouse model of infection despite the improved growth rate *in vitro*. Our findings suggest that the CarD-RNAP interaction protects CarD from proteolytic degradation in *M. tuberculosis*, establish that growth rate and rRNA levels can be uncoupled in *M. tuberculosis* and demonstrate that the strength of the CarD-RNAP interaction has been finely tuned to optimize virulence.

IMPORTANCE *Mycobacterium tuberculosis*, the causative agent of tuberculosis, remains a major global health problem. In order to develop new strategies to battle this pathogen, we must gain a better understanding of the molecular processes involved in its survival and pathogenesis. We have previously identified CarD as an essential transcriptional regulator in mycobacteria. In this study, we detail the effects of increasing the affinity of CarD for RNAP on transcriptional regulation, CarD protein stability, and virulence. These studies expand our understanding of the global transcription regulator CarD, provide insight into how CarD activity is regulated, and broaden our understanding of prokaryotic transcription.

KEYWORDS *Mycobacterium tuberculosis*, RNA polymerase, protein stability, protein-protein interactions, rRNA, transcription initiation factor

Received 22 September 2016 **Accepted** 23 November 2016

Accepted manuscript posted online 5 December 2016

Citation Garner AL, Rammohan J, Huynh JP, Onder LM, Chen J, Bae B, Jensen D, Weiss LA, Manzano AR, Darst SA, Campbell EA, Nickels BE, Galburt EA, Stallings CL. 2017. Effects of increasing the affinity of CarD for RNA polymerase on *Mycobacterium tuberculosis* growth, rRNA transcription, and virulence. J Bacteriol 199:e00698-16. https://doi.org/10.1128/JB.00698-16.

Editor Tina M. Henkin, Ohio State University

Address correspondence to Christina L. Stallings, stallings@wustl.edu.

Mycobacterium tuberculosis remains a major global health problem, resulting in 9.6 million new cases of tuberculosis (TB) in 2014 and 1.5 million TB-related deaths that year (1). Control of the *M. tuberculosis* epidemic is hampered by the increasing prevalence of multidrug-resistant strains, which resulted in 480,000 patients developing

multidrug-resistant TB in 2014. In order to develop new strategies to battle this pathogen, we must gain a better understanding of the molecular processes involved in its survival and pathogenesis. Recent studies have identified numerous aspects of mycobacterial physiology that differ from what has been identified in model organisms and highlight the importance of research directly in mycobacteria to understand their lineage specific physiology. We have identified CarD as an essential transcriptional regulator in mycobacteria that is not conserved in the model organism *Escherichia coli*, which has traditionally been used to study mechanisms of transcription (2). *carD* is conserved in all mycobacteria and numerous other bacteria (2–5) but is not found in eukaryotes. Therefore, studying CarD will broaden our understanding of prokaryotic transcription while also characterizing a promising potential target for desperately needed new therapeutic strategies for TB.

Chromatin immunoprecipitation-sequencing (ChIP-seq) experiments in mycobacteria demonstrated that CarD is localized with RNA polymerase (RNAP) holoenzyme at promoters throughout the genome, indicating that CarD is a global regulator of transcription initiation (4). CarD interacts directly with the β1 lobe of the RNAP-β subunit through its N-terminal RNAP interaction domain (RID) (2, 5, 6) and with DNA just upstream of the −10 element of the promoter through a conserved basic patch in its C-terminal domain (3, 4, 7). Within the basic patch, studies have identified a highly conserved tryptophan residue that is proposed to wedge into the minor groove at the upstream edge of the transcription bubble (3, 4). Thus far, CarD's activity has primarily been studied on rRNA promoters. Using *in vitro* transcription assays, we have shown that CarD stabilizes RNAP-promoter open complexes at rRNA promoters during transcription initiation and that CarD requires interactions with both RNAP and DNA, as well as the activity of the conserved tryptophan to do so (4, 6–8). Recently, a bulk fluorescence assay was used to measure the effect of CarD on the kinetics of transcription initiation at the *M. tuberculosis* rRNA promoter *rrnA*P3. These studies revealed that, compared to the *Escherichia coli* RNAP, the *Mycobacterium bovis* RNAP forms a significantly less stable open complex at *rrnA*P3 in the absence of CarD. Addition of CarD stabilizes *M. bovis* RNAP-*rrnA*P3 open complexes by binding to the RNAP-promoter open complex with high affinity and preventing collapse to closed complex. With lower affinity, CarD also binds the RNAP-promoter closed complex and promotes melting of the DNA to form open complex. Importantly, the cellular concentration of CarD in wild-type (WT) *M. tuberculosis* is sufficient for both of these activities to be physiologically relevant (8). Mycobacterial strains expressing mutants of CarD with weakened affinity for the RNAP-β subunit, weakened affinity for DNA, or that are mutated at the conserved tryptophan all express lower levels of rRNA exhibit lower rRNA promoter activation in promoter-*lacZ* fusion experiments, grow slower, and are more sensitive to multiple stresses and antibiotics compared to strains expressing WT CarD (4, 6, 7).

In this study, we use CarD mutants with increased affinity for RNAP to dissect the role of CarD binding to RNAP *in vitro* and *in vivo*. We detail the distinct effects of increasing the affinity of CarD for RNAP on open complex stability, transcriptional regulation, CarD protein stability, and the effects of these changes on growth and virulence. These studies expand our understanding of the global transcription regulator CarD and the impact of CarD activity on the physiology of *M. tuberculosis*, while also providing insight into how CarD activity is regulated.

RESULTS

Identification of amino acid substitutions in the N terminus of CarD that increase the affinity of CarD for RNAP-β. To identify substitutions that strengthen the *M. tuberculosis* CarD/RNAP-β β1 lobe interaction, we used site-directed mutagenesis guided by a comparison between our X-ray structure of *Thermus thermophilus* CarD in complex with the β1 lobe of *T. thermophilus* RNAP (Protein Data Bank [PDB] accession no. 4XAX) (3) (Fig. 1A), solved to 2.4-Å resolution, and the structure of *M. tuberculosis* CarD in complex with the RNAP-β β1 and β2 lobes of *M. tuberculosis* RNAP (PDB accession no. 4KBM) (9), solved to 2.11 Å. The β1 lobes from each structure were

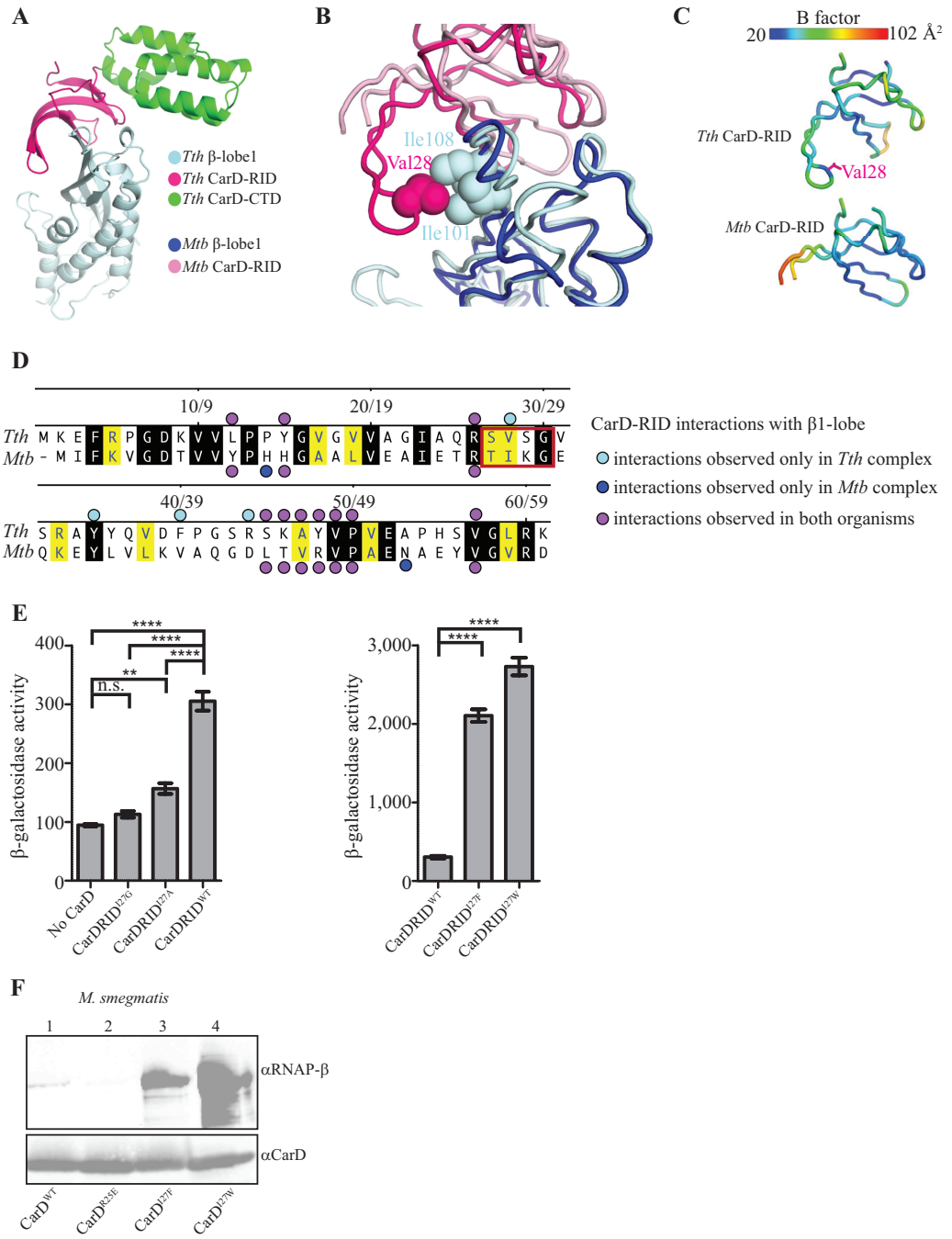

FIG 1 Single point mutations in CarD specifically increase CarD's affinity for RNAP-β. (A) Crystal structure of *T. thermophilus* CarD in complex with the β1 lobe of *T. thermophilus* RNAP reveals molecular interactions between the two proteins at high-resolution (2.4-Å) detail. CTD, C-terminal domain. (B) Structural alignment of the β1 lobes of *T. thermophilus* CarD:β1-lobe and *M. tuberculosis* CarD:β1-lobe structures to compare the interactions between the CarD RID and RNAP β1 in each organism. (C) Atom displacement was rendered visually using PyMOL B-factor rendering. The spectrum scale above illustrates a range of low B-factors (highly ordered, blue indicates under 30%) to high B-factors (disordered, red indicates 90% or higher). (D) Alignment of *T. thermophilus* (top) and *M. tuberculosis* (bottom) CarD RIDs comparing interactions with their cognate RNAP β1 lobe. Black shading indicates residues that are identical and yellow shading indicates residues that are homologous. The following groups are considered homologous: R and K; E and D; V, I, L, M, and A; S and T; and Q and N. Bullets are defined in the figure by interactions unique to each organism or shared by both. The red box designates the region that is observed in the *T. thermophilus* complex but not the *M. tuberculosis* complex. (E) Results of β-Gal assays (6, 15) examining the effects of amino acid substitutions at position 27 of the *M. tuberculosis* CarD RID on the interaction between the *M. tuberculosis* CarD RID and the *M. tuberculosis* β1 lobe. The bar graphs show β-Gal activity in Miller units observed in assays done using cells containing the indicated *M. tuberculosis* CarD RID derivative and the *M. tuberculosis* β1 lobe, as well as assays performed using cells containing only the *M. tuberculosis* β1 lobe. Each graph shows the means ± the SEM of data from five replicates. Statistical significance was analyzed by analysis of variance (ANOVA) and Tukey's multiple-comparison test (n.s., not significant; **, $P \leq 0.01$; ****, $P \leq 0.0001$). (F) Immunoprecipitation experiments with a

(Continued on next page)

aligned over 919 atoms in PyMOL (version 1.8; Schrödinger, LLC) to give a root mean square (RMS) of 1.095 Å, and the interactions between the β1 lobe and the CarD RID were compared. Many of the interactions were conserved between the *T. thermophilus* and *M. tuberculosis* structures (Fig. 1B and D), but a significant difference was noted in a region that included a loop at the tip of the RID (residues 26 to 29 in *M. tuberculosis*) that was not modeled in the *M. tuberculosis* structure, presumably due to a lack of density. Cartoon rendering by B-factors (PyMOL) of both structures revealed that this loop was highly disordered in *M. tuberculosis* but well ordered in *T. thermophilus*, presumably due to its interaction with the β1 lobe (Fig. 1C). In particular, the *T. thermophilus* structure revealed a nonpolar interaction between loop residue V28 from CarD (I27 in *M. tuberculosis*) and I101 and I108 from the β1 lobe (I140 and I147 in *M. tuberculosis*) that was not visible in the *M. tuberculosis* structure due to disorder (Fig. 1B). Based on the *T. thermophilus* structure of the β1 lobe in complex with CarD, we predicted that the isoleucine side chain at position 27 of *M. tuberculosis* CarD likely contributes to an interaction between the *M. tuberculosis* CarD RID and the *M. tuberculosis* β1 lobe that may not have been observed in the crystal structure due to crystal packing constraints. Furthermore, structural modeling predicts that removal of the isoleucine side chain at position 27 of the *M. tuberculosis* CarD RID would weaken the interaction between the *M. tuberculosis* CarD RID and the *M. tuberculosis* β1 lobe, whereas substitutions of position 27 with residues containing side chains that are more hydrophobic than isoleucine might strengthen the interaction between the *M. tuberculosis* CarD RID and the *M. tuberculosis* β1 lobe.

To test these predictions, we used an *E. coli*-based bacterial two-hybrid assay that detects the interaction between the *M. tuberculosis* CarD RID and the *M. tuberculosis* β1 lobe (6). In this assay, the interaction between the WT *M. tuberculosis* CarD RID (amino acids 1 to 66) and the *M. tuberculosis* β1 lobe results in a 3-fold increase in β-galactosidase (β-Gal) activity from the two-hybrid test promoter (Fig. 1E). Substitution of I27 of the CarD RID with alanine or glycine reduced the β-Gal activity to near background levels, while substitution of I27 of the CarD RID with the bulkier hydrophobic residues phenylalanine and tryptophan resulted in 7- and 9-fold increases, respectively, in β-Gal activity relative to that observed with the WT *M. tuberculosis* CarD RID (Fig. 1E). The results of the two hybrid assays indicate that I27A and I27G substitutions weaken the interaction between the *M. tuberculosis* CarD RID and the *M. tuberculosis* β1 lobe whereas I27F and I27W substitutions strengthen the interaction between the *M. tuberculosis* CarD RID and the *M. tuberculosis* β1 lobe, a finding consistent with the predictions from the structural modeling.

To determine whether the CarD I27F and I27W mutations increase the affinity of the interaction between CarD and RNAP-β subunit *in vivo*, we constructed *Mycobacterium smegmatis* strains expressing hemagglutinin (HA)-tagged wild-type CarD ($CarD^{WT}$), CarD with an R-to-E change at position 25 ($CarD^{R25E}$), $CarD^{I27F}$, or $CarD^{I27W}$. Coimmunoprecipitation experiments in *M. smegmatis* demonstrated that $CarD^{I27W}$ and $CarD^{I27F}$ mutants coprecipitated more RNAP-β than $CarD^{WT}$ (Fig. 1F). As previously reported, the $CarD^{R25E}$ mutant, which has lower affinity for RNAP-β than $CarD^{WT}$, coprecipitated less RNAP-β than $CarD^{WT}$ (6). The $CarD^{I27W}$ mutant associated with more RNAP-β than $CarD^{I27F}$, indicating a higher-affinity interaction.

$CarD^{I27F}$ and $CarD^{I27W}$ mutants stabilize open complexes at lower concentrations than $CarD^{WT}$. CarD regulates transcription initiation by binding to and stabilizing RNAP-promoter open complexes (3, 4, 7, 8, 10). We have previously developed a fluorescence assay for CarD activity that reports on open complex formation in real-time. In this assay, a Cy3 label, which exhibits a 2-fold fluorescence enhancement in open complex, is incorporated at the +2 position on the nontemplate strand of the *M.*

FIG 1 Legend (Continued)
monoclonal antibody specific for HA in the *M. smegmatis* Δ*carD attB*::*tet-carD* strain expressing *M. tuberculosis* $CarD^{WT}$-HA (lane 1), $CarD^{R25E}$-HA (lane 2), $CarD^{I27F}$-HA (lane 3), or $CarD^{I27W}$-HA (lane 4). Immunoprecipitated eluates were analyzed by Western blotting with monoclonal antibodies specific for either RNAP-β or CarD.

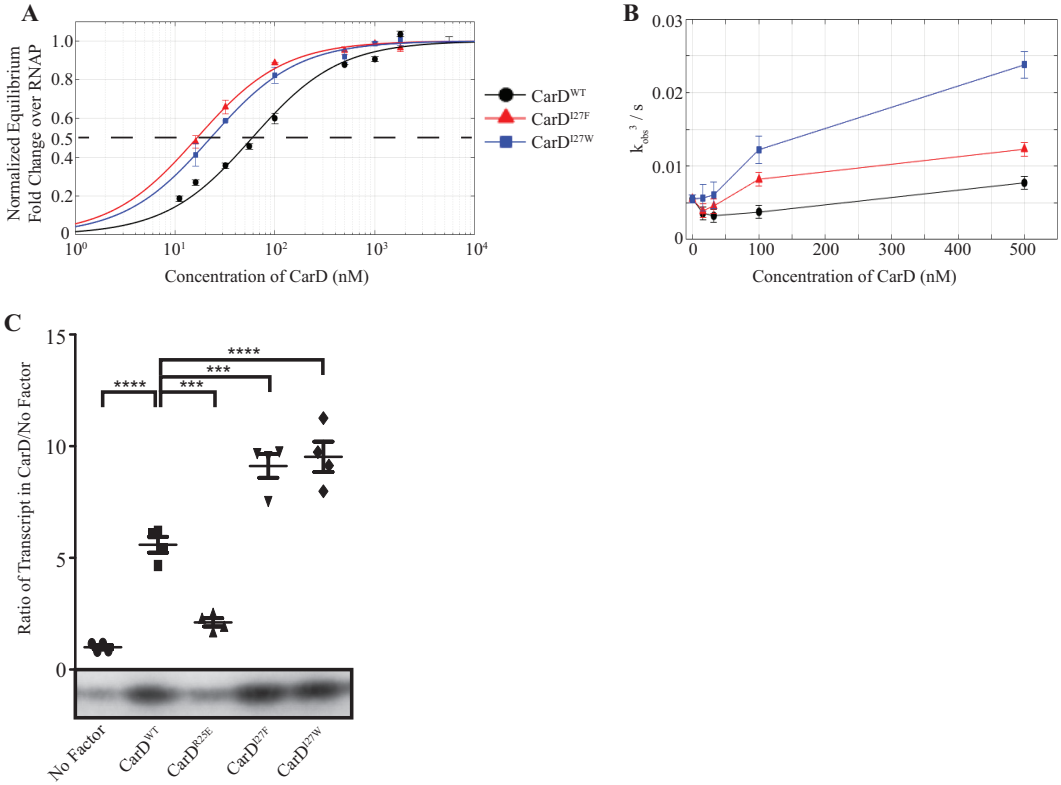

FIG 2 Effects of increasing the affinity of CarD for RNAP on open complex stability. (A) Equilibrium fluorescence fold change normalized to the fold change at high CarD concentrations (saturation) for each mutant of CarD with 225 nM *M. bovis* RNAP-σ^A and 10 nM Cy3-labeled *M. tuberculosis rrnA*P3 promoter. Both *M. tuberculosis* CarD^{I27F} (red) and CarD^{I27W} (blue) mutants achieve a half-maximal effect (dashed line) at lower concentrations (17 ± 2 nM for CarD^{I27F} and 23 ± 3 nM for CarD^{I27W}) than *M. tuberculosis* CarD^{WT} (black; 59 ± 10 nM). (B) $k_{obs}{}^3$ values, calculated using ProData Viewer software from Applied Photophysics, of open complex formation as a function of CarD concentration for *M. tuberculosis* CarD^{WT} (black), CarD^{I27F} (red), and CarD^{I27W} (blue). (C) *In vitro* transcription assay results showing a representative gel and a graph of the ratio of the amount of 3-nt initial transcript formed by 200 nM *M. bovis* RNAP-σ^A from 10 nM a linear DNA fragment in the presence of 2 μM CarD versus in the absence of CarD for reaction mixtures containing no CarD, *M. tuberculosis* CarD^{WT}, CarD^{R25E}, CarD^{I27F}, or CarD^{I27W}. The graph shows the means ± the SEM of data from at least four replicates. Statistical significance was analyzed by ANOVA and Tukey's multiple-comparison test (***, $P \leq 0.001$; ****, $P \leq 0.0001$).

*tuberculosis rrnA*P3 promoter within a linear fragment of *M. tuberculosis* genomic DNA containing nucleotides 1470151 to 1470300 (8). *M. bovis* RNAP-σ^A holoenzyme with or without *M. tuberculosis* CarD is then mixed with the labeled DNA fragment via stopped-flow spectrophotometry, and the fluorescence is monitored for 20 min. The Cy3 label increases fluorescence in the open complex conformation, and thus the rate of open complex formation can be monitored as a change in fluorescence. The amplitude of the fluorescence intensity curve correlates to the equilibrium amount of open complex in a given condition (8). To monitor the effect of increasing the affinity of CarD for RNAP on the formation and stability of open complexes, we performed this assay with concentrations of CarD^{I27F} and CarD^{I27W} ranging for 0 to 1800 nM and fixed concentrations of RNAP (225 nM) and promoter DNA (10 nM) (Fig. 2A). We found that the CarD concentration necessary to reach half of the maximum level of open complex at saturation (half-maximal concentration) was lower for CarD^{I27F} (17 ± 2 nM) and CarD^{I27W} (23 ± 3 nM) than for CarD^{WT} (59 ± 10 nM), which is consistent with a higher affinity of the CarD I27 mutants for RNAP in initiation complexes compared to CarD^{WT} (Fig. 2A).

CarD^{I27F} and CarD^{I27W} mutants accelerate promoter opening at lower concentrations than CarD^{WT}. We have previously reported modeling based on the trends of the slowest observed rate in the real-time fluorescent traces ($k_{obs}{}^3$) that suggests that CarD stabilizes open complex through a two-tiered concentration-dependent mechanism where CarD associates with both open and closed complexes with different

affinities (8). More specifically, the model predicts that at low concentrations (i.e., <100 nM), CarD^{WT} binds to open complex and prevents bubble collapse, resulting in more open complex and a slower observed rate. The model further predicts that at higher concentrations, CarD^{WT} binds to the closed complex and accelerates the rate of opening, resulting in still more open complex and an acceleration in the observed rate. Analysis of k_{obs}^3 as a function of CarD concentration was performed for the CarD I27 mutants as previously described (8) (Fig. 2B). We found that the I27 mutants begin to accelerate k_{obs}^3 at lower concentrations (<50 nM) than WT CarD (100 nM). In fact, for CarD^{I27W} we did not observe a deceleration in k_{obs}^3 even at the lowest concentration tested (16 nM). The two-tiered kinetic model predicts that acceleration in k_{obs}^3 arises from CarD binding to closed complex, which increases the rate of promoter opening. Thus, our working model predicts that, even at 16 nM, CarD^{I27W} is associating with closed complex and accelerating opening. The acceleration of the observed rate at lower concentrations coupled with the lower half-maximal concentration for open complex stabilization is consistent with a model where the CarD I27 mutants have higher affinities to both closed and open RNAP-promoter complexes compared to CarD^{WT}.

Increasing the affinity of CarD for RNAP increases formation of initial RNA products. To investigate whether increasing the affinity of CarD for RNAP affects RNA synthesis, we monitored initial product formation in a multiround *in vitro* transcription assay (10). *M. bovis* RNAP-σ^A holoenzyme was incubated with the promoter template used in the fluorescence assays, but without the Cy3 label, in the presence or absence of WT or mutant *M. tuberculosis* CarD. GpU dinucleotide was used as the initiating nucleotide, and radiolabeled UTP was added as the extending nucleotide. Reaction mixtures were incubated for 20 min, after which the amounts of initial trinucleotide RNA products (GpUpU) were quantified. Addition of CarD^{WT} protein increases the amount of initial RNA product formation ~6-fold compared to the amount of product produced in the absence of CarD (Fig. 2C), whereas CarD^{R25E}, which has decreased affinity for RNAP, only increases the amount of product formed ~2-fold. In contrast, CarD^{I27F} and CarD^{I27W} increase the amount of product formed ~9-fold. These data demonstrate that increasing the affinity of CarD for the RNAP results in an increase in initial RNA product formation. We infer that the effect of strengthening the interaction between CarD and RNAP on initial RNA product formation is a consequence of an increase in the formation of RNAP-promoter complexes (Fig. 2).

Increasing the affinity of CarD for RNAP stabilizes the CarD protein in *M. tuberculosis*. In previous work, we constructed a strain of *M. tuberculosis* in which a copy of *carD* is expressed from a constitutive promoter at the *attB* site, a nonendogenous chromosomal locus, and the endogenous copy of *carD* is deleted (2). We have previously shown that a strain of *M. tuberculosis* that expresses *carD^{R47E}*, which encodes a CarD protein that has an R-to-E change at position 47 and weakened affinity for the RNAP, from the *attB* site grows more slowly than a strain expressing wild-type *carD* (*carD^{WT}*) from the *attB* site (6). To determine the effects of increasing the affinity of CarD for RNAP in the bacteria, we constructed *M. tuberculosis* strains expressing *carD^{I27F}* or *carD^{I27W}* from the *attB* site. We first determined the expression levels of the *carD* alleles in each strain by measuring *carD* transcript and protein levels. We found the CarD^{WT}, CarD^{I27F}, CarD^{I27W}, and CarD^{R47E} strains all produce equal levels of *carD* transcript, as expected given that the strains express the *carD* gene from the same promoter (Fig. 3A). However, when we examined the protein content in these strains we found that the CarD^{I27F} and CarD^{I27W} strains reproducibly had more CarD protein than the CarD^{WT} strain (Fig. 3B, RNAP β levels also shown as a loading control). In addition, this effect is proportional to the magnitude of the change in affinity, since the CarD^{I27W} strain reproducibly has more CarD protein than the CarD^{I27F} strain and the CarD^{WT} strain has more CarD protein than CarD^{R47E}. Given the equal amount of transcript being produced, the different levels of protein indicate posttranslational differences in the stability of CarD protein in these strains. CarD has previously been identified as a Clp protease substrate in *M. tuberculosis* (11). Taken together, our data can be explained in

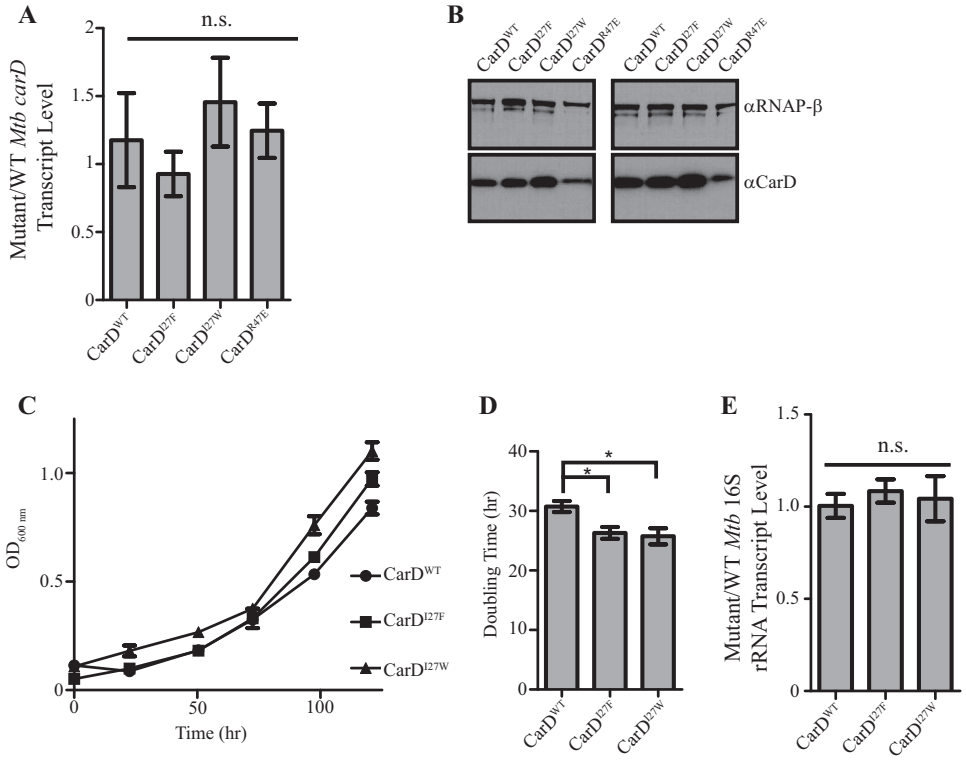

FIG 3 Increasing CarD's affinity for RNAP results in more stable CarD protein and faster growth without a change in rRNA levels. (*A*) The ratio of *carD* transcript levels in exponential cultures of the Δ*carD attB*::*tet-carD* strain expressing CarD^{I27F}, CarD^{I27W}, or CarD^{R47E} to levels in the CarD^{WT} strain when grown in Sauton's medium. Transcript levels were determined using qRT-PCR and normalized to *sigA*. (B) Western blot analysis results of two biological replicates of lysates from the same cultures as used in panel A. Membranes were blotted with a monoclonal antibody against RNAP-β (top) or a polyclonal antibody against CarD (bottom). RNAP-β was used as a loading control for each sample. (C) Representative growth curves of the Δ*carD attB*::*tet-carD* strain expressing CarD^{WT}, CarD^{I27F}, or CarD^{I27W} in Sauton's medium. (D) Doubling times of the Δ*carD attB*::*tet-carD* strain expressing CarD^{WT}, CarD^{I27F}, or CarD^{I27W} in Sauton's medium. Doubling times were calculated for each of five biological replicate growth curves using the exponential growth equation and excluding values after the optical density at 600 nm (OD_{600}) reached 1 to focus on the growth rate in the exponential growth phase. (E) Ratio of 16S rRNA levels in exponential cultures of the Δ*carD attB*::*tet-carD* strain expressing CarD^{I27F} or CarD^{I27W} to levels in the CarD^{WT} strain when grown in Sauton's medium. Transcript levels were determined using qRT-PCR and normalized to *sigA*. Each graph shows the means ± the SEM of data from at least three replicates. Statistical significance was analyzed by ANOVA and Tukey's multiple-comparison test (n.s., not significant; *, $P \leq 0.05$).

the context of a model where CarD is protected from proteolysis when associated with RNAP.

Increasing CarD's affinity for RNAP increases the growth rate in *M. tuberculosis*. We have previously reported that decreasing CarD's affinity for RNAP decreases growth rate in *M. tuberculosis* strain (6). To determine the effect of increasing CarD's affinity for RNAP on growth rate, we back-diluted cultures in the exponential growth phase (to avoid an initial lag phase) into fresh liquid Sauton's medium and monitored growth. We found that the CarD^{I27F} and CarD^{I27W} strains had a faster doubling time than the CarD^{WT} stain (26.31-, 25.75-, and 30.74-h doubling times, respectively) (Fig. 3C and D). These results, as well as the growth defect previously reported in a strain expressing a CarD mutant with lower affinity for RNAP (6), demonstrate that the affinity of CarD for the RNAP can impact growth rate in *M. tuberculosis*.

Increasing the affinity of CarD for RNAP does not result in differences in rRNA transcript levels in *M. tuberculosis*, despite the effects on growth rate. We have previously shown that decreasing the affinity of CarD for RNAP results in decreased rRNA levels and slower growth (6, 7). Because rRNA levels are often correlated to growth rate (12–14), the decreased rRNA levels in the CarD mutants with lower affinity for RNAP could contribute to the growth defect associated with these mutations. To

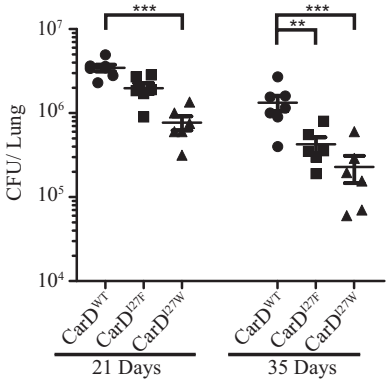

FIG 4 Increasing CarD's affinity for RNAP attenuates *M. tuberculosis* in a mouse model of infection. Dot plot of CFU in the lungs of C57BL/6J mice infected with the Δ*carD attB*::*tet-carD* strain expressing either CarD^{WT} (●), CarD^{I27F} (■), or CarD^{I27W} (▲). Each time point is the means ± the SEM of data from at least six mice per strain. Statistical significance was analyzed by ANOVA and Tukey's multiple-comparison test (**, $P \leq 0.01$; ***; $P \leq 0.001$). All comparisons were tested, and only significantly different comparisons are shown.

determine the effect of increasing the affinity of the interaction between CarD and RNAP on rRNA levels in the bacterium, we isolated RNA from exponential cultures of CarD^{WT}, CarD^{I27F}, and CarD^{I27W} strains in Sauton's medium and performed quantitative real-time PCR (qRT-PCR) analysis for the levels of stable 16S rRNA using primers internal to the 16S rRNA transcript (Fig. 3E). The CarD I27 mutants that have higher affinity for RNAP express the same amount of rRNA as the CarD^{WT} strain, indicating that the faster growth in these strains is not a result of increasing rRNA expression. Therefore, the rRNA levels and growth rate are uncoupled in strains expressing CarD proteins with various affinities to RNAP. Thus, the effects of altering CarD's affinity for RNAP on growth rate can occur independently of effects on rRNA levels. To the best of our knowledge, this is also the first report of rRNA levels and growth rate being uncoupled in *M. tuberculosis*.

Increasing the affinity of CarD for RNAP attenuates survival of *M. tuberculosis* during infection of mice. We have previously shown that weakening the interaction of CarD with RNAP results in decreased bacterial survival by 35 days postinfection (dpi) in mice (6). To determine the effect of increasing the affinity of CarD for RNAP on virulence, we infected C57BL/6J mice with the *M. tuberculosis* CarD^{WT}, CarD^{I27F}, or CarD^{I27W} strains and measured the bacterial burden in the lungs at 21 and 35 dpi (Fig. 4). Both the CarD^{I27F} and the CarD^{I27W} mutants were attenuated for survival in the mice and displayed significantly lower bacterial burden in the lungs (Fig. 4). Specifically, the CarD^{I27W} strain displayed significantly lower bacterial burden than the CarD^{WT} strain at 21 and 35 dpi, whereas the CarD^{I27F} strain had lower bacterial burdens than CarD^{WT} at 35 dpi. The severity of the virulence defect in the CarD mutants mirrors the effect of these mutations on the affinity of CarD for RNAP, with CarD^{I27W} exhibiting both a higher affinity and a more pronounced virulence defect than CarD^{I27F}. These data show that although increasing the affinity of CarD for RNAP increases the rate of formation of transcription competent RNAP-promoter complexes and increases growth rates in culture, it results in a loss of virulence. The degree of attenuation at 35 dpi for the CarD I27 mutants is similar to that previously reported for *M. tuberculosis* strains expressing a mutant CarD protein with lower affinity for the RNAP (6). Thus, either decreasing or increasing the affinity of CarD for RNAP has a detrimental effect on the virulence of *M. tuberculosis*. We therefore propose that this indicates that the affinity of CarD for RNAP is finely tuned to the physiology of this obligate pathogen to optimize virulence.

DISCUSSION

In this study, we investigated both the biochemical and the physiological effects of increasing the affinity of CarD for RNAP. Our findings reveal new aspects of CarD

regulation and the effect of increasing the affinity of CarD for RNAP-β on growth rate and virulence.

Using a real-time fluorescence assay, we found that increasing the affinity of CarD for RNAP leads to a decrease in the concentration of CarD required for half-maximal open complex formation and stability (Fig. 2A). Our data further show that the higher-affinity CarD mutants result in increased stability of an RNAP-promoter complex and an increase in the formation of initial RNA products (Fig. 2C). However, despite these positive effects of the CarD I27 mutants on the formation of transcription competent RNAP-promoter complexes at *rrnA*P3 *in vitro*, *M. tuberculosis* strains expressing CarD^{I27F} or CarD^{I27W} did not contain higher levels of rRNA than the CarD^{WT} strain (Fig. 3E). This observation may be explained by the presence of other factors *in vivo* that impact whether rRNA levels respond to changes in the affinity of CarD for the RNAP. In addition, increasing the affinity of CarD for RNAP-β may affect other stages of transcription after open complex formation (i.e., promoter escape) that ultimately impact full transcript production. These possibilities will be explored in future investigations.

We found that increasing the affinity of CarD for RNAP results in an increase in growth rate without changing the levels of rRNA (Fig. 3C and D). This suggests that in WT strains rRNA and ribosomes would be in excess of the amounts required to accommodate a higher growth rate. We also found that increasing the affinity of CarD for RNAP in *M. tuberculosis* results in attenuated virulence in mice (Fig. 4). Together, these findings demonstrate that the differences in growth rate and virulence of the CarD I27 mutant strains are not a result of altered rRNA content but are instead another consequence of varied levels or activity of CarD proteins, thus uncoupling the role of CarD in regulating rRNA content from its effect on growth rate. Therefore, the essential function of CarD is unlikely to be limited to regulation of rRNA levels. These data also indicate that there exist non-rRNA genes that are more sensitive to changes in the affinity of CarD for RNAP than the rRNA genes. We have previously shown that in the absence of CarD, the mycobacterial RNAP is only weakly able to form open complexes at *rrnA*P3 (3, 8, 10). In addition, CarD is localized to promoter-bound RNAP holoenzymes throughout the genome (4). These studies suggest that CarD may in fact be a general component of the transcription initiation machinery in mycobacteria and that its essential role is enabling the mycobacterial RNAP to efficiently form open complexes at all promoters in the genome. In particular, changes in the affinity of CarD for the RNAP could result in a global dysregulation of gene expression. Alternatively, phenotypes of CarD mutants may result from the deregulation of a specific subset of genes differentially regulated by CarD. It should also be noted that, despite the presence at all promoters, at this point CarD activity has only been evaluated at mycobacterial rRNA promoters and consensus promoters from *E. coli*. Therefore, a priority of future work will be to clarify the role of CarD in global transcription regulation.

Using multiple CarD mutants, we have also revealed a role for the CarD-RNAP interaction in regulating CarD protein levels. Increasing the affinity of CarD for RNAP increases the cellular concentration of CarD without affecting *carD* transcript levels (Fig. 3A and B). The effect on CarD protein concentration is proportional to the affinity for RNAP and, of the strains expressing *carD* from the *attB* site, CarD^{I27W} has the highest affinity for RNAP and the highest concentration of CarD protein, while CarD^{R47E} has the lowest affinity for CarD and the lowest CarD protein levels (Fig. 3A and B). These data suggest that CarD is protected from proteolytic degradation while associated with RNAP. Since CarD is a known target of the Clp protease in mycobacteria (11), one possibility is that Clp-mediated degradation of CarD is more efficient when CarD is not associated with RNAP. Thus, our findings provide a mechanistic explanation for our previous observation that mycobacteria contain a similar concentration of CarD and the housekeeping sigma factor (8) and suggest that there may be a detrimental effect of excess, free cellular CarD.

MATERIALS AND METHODS

Bacterial two-hybrid assays. The bacterial two-hybrid assay used in this study is based upon the demonstration that contact between a protein domain fused to the α subunit of RNA polymerase and

a partner protein fused to the bacteriophage λCI protein activates transcription of a *lacZ* reporter gene under the control of a test promoter bearing an upstream λ operator (15). Assays were performed as described using *E. coli* FW102 F′ O_L2-62 reporter strain cells, which contain the test promoter placO_L2-62 driving the expression of a linked *lacZ* gene on an F′ episome (15). Plasmids used in these assays included pBRα-Mt CarD (1 to 66), which encodes residues 1 to 248 of the *E. coli* RNAP α subunit fused to residues 1 to 66 of *M. tuberculosis* CarD (6); plasmid pBRα, which encodes the WT α subunit; and plasmid pACλCI-Mt β1, which encodes residues 1 to 236 of the bacteriophage λCI protein fused to residues 52 to 178 of the β subunit of *M. tuberculosis* RNAP fused to residues 379 to 440 of the β subunit of *M. tuberculosis* RNAP via two glycine residues (6). Plasmids carrying amino acid substitutions at residue I27 of *M. tuberculosis* CarD were introduced into pBRα-CarD (1 to 66) by PCR.

FW102 F′ O_L2-62 were cotransformed with either the indicated pBRα-Mt CarD (1 to 66) derivative and pACλCI-Mt β1 or pBRα and pACλCI-Mt β1. Individual transformants were selected and grown in Luria-Bertani (LB) medium supplemented with carbenicillin (100 μg/ml), chloramphenicol (25 μg/ml), and kanamycin (50 μg/ml). No IPTG (isopropyl-β-D-thiogalactopyranoside) was present in the growth medium. β-Galactosidase assays were performed as described previously (6). Graphs in Fig. 1E depict the β-Gal activity in cells containing the indicated pBRα-Mt CarD (1 to 66) derivative and pACλCI-Mt β1. The bar labeled "No CarD" in Fig. 1E depicts the β-Gal activity observed in cells containing pBRα and pACλCI-Mt β1.

Bacterial strains and growth conditions. (i) *M. tuberculosis*. All *M. tuberculosis* strains were derived from the Erdman strain and were grown at 37°C in Sauton's broth medium (0.5 g liter^{-1} KH_2PO_4, 0.5 g liter^{-1} $MgSO_4$, 4 g liter^{-1} L-asparagine, 60 ml of glycerol, 0.05 g liter^{-1} ferric ammonium citrate, 2.0 g liter^{-1} citric acid, 0.1 ml liter^{-1} 1% $ZnSO_4$, 0.05% Tween 80 [pH 7.0]) or 7H10 agar medium (Difco) supplemented with 60 μl liter^{-1} oleic acid, 5 g liter^{-1} bovine serum albumin (BSA), 2 g liter^{-1} dextrose, 0.003 g liter^{-1} catalase (OADC), and 0.5% glycerol. Gene switching was used to construct strains of mycobacteria expressing different *carD* alleles and to test for their viability (6, 16). Specifically, the *M. tuberculosis* Δ*carD attB*::*tet-carD* strain (described previously in reference 2) was transformed with pMSG430*Rv3583c*^{I27F}, pMSG430*Rv3583c*^{I27W}, or pMSG430*Rv3583c*^{R47E} (expresses *M. tuberculosis* CarD^{WT}, CarD^{I27F}, CarD^{I27W}, or CarD^{R47E}, respectively, from a constitutive P*myc1-tetO* promoter, kanamycin resistant) or pDB19Rv3583c (expresses CarD^{WT} from a constitutive P*myc1-tetO* promoter, zeocin resistant). The transformants were selected on 20 μg ml^{-1} kanamycin or 1.25 μg ml^{-1} zeocin. The *carD* gene from each transformant was sequenced to confirm the presence of the correct sequence. The *M. tuberculosis* Δ*carD attB*::*tet-carD* strains transformed with pDB19*Rv3583c*^{WT}, pMSG430*Rv3583c*^{I27F}, pMSG430*Rv3583c*^{I27W}, or pMSG430*Rv3583c*^{R47E} were named mgm3080, csm230, csm231 and csm195, respectively.

(ii) *M. smegmatis*. All *M. smegmatis* strains were derived from mc^{2}155 and were grown at 37°C in LB medium supplemented with 0.5% dextrose, 0.5% glycerol, and 0.05% Tween 80 (broth). *M. smegmatis* strains expressing HA-tagged CarD^{WT}, CarD^{R25E}, CarD^{I27F}, or CarD^{I27W} were engineered as described for the analogous *M. tuberculosis* strains using pMSG430 expression plasmids and the *M. smegmatis* Δ*carD attB*::*tet-carD* strain (described previously in reference 2). The *M. smegmatis* Δ*carD attB*::*tet-carD* strains expressing C-terminal HA-tagged versions of *M. tuberculosis* CarD^{WT}, *M. tuberculosis* CarD^{R25E}, *M. tuberculosis* CarD^{I27F}, or *M. tuberculosis* CarD^{I27W} from a constitutive P*myc1-tetO* promoter at the *attB* site of *M. smegmatis* Δ*carD attB*::*tet-carD* were named mgm3090, mgm3091, csm228, and csm229, respectively.

Cell lysate. Next, 20-ml portions of exponential cultures of *M. tuberculosis* were lysed in 500 μl of NP-40 buffer (10 mM sodium phosphate [pH 8.0], 150 mM NaCl, and 0.25% NP-40) by bead beating three times.

Immunoprecipitation. Lysate from *M. smegmatis* strains expressing HA-tagged alleles of CarD was bound to monoclonal anti-HA–agarose (Sigma), and the complexes were eluted as previously described (6, 7).

Western blot analysis. Protein samples were mixed with an SDS-PAGE loading buffer and run on a 4 to 12% Bis-Tris protein gel (Invitrogen). HA-tagged CarD in the immunoprecipitation experiment was detected using a mouse monoclonal antibody (clone 10F05; Memorial Sloan-Kettering Cancer Center Monoclonal Antibody Core Facility). To determine protein concentrations in cell lysate, CarD was detected with a rabbit polyclonal antibody (2). RNAP-β was detected with a mouse monoclonal antibody in both experiments (clone 8RB13; Neoclone, Madison, WI). Horseradish peroxidase-conjugated secondary antibodies against mouse or rabbit (Perkin-Elmer) were used for detection.

Quantitative real-time PCR. RNA was prepared from 20 to 30 ml of *M. tuberculosis* Erdman (WT *M. tuberculosis*), mgm3080 (CarD^{WT}), csm195 (CarD^{R47E}), csm230 (CarD^{I27F}), and csm231 (CarD^{I27W}) during the exponential growth phase. 16S rRNA and *carD* levels were measured and normalized to *sigA* transcript levels as previously described (2).

Mouse infections. Infection of mice with exponentially replicating *M. tuberculosis* Erdman strain (WT *M. tuberculosis*), csm3080 (CarD^{WT}), csm230 (CarD^{I27F}), and csm231 (CarD^{I27W}) strains and the determination of bacterial loads were performed as previously described (6, 7). All procedures involving animals were conducted according to the National Institutes of Health (NIH) guidelines for the housing and care of laboratory animals, and all procedures were performed in accordance with institutional regulations after protocol review and approval by the Institutional Animal Care and Use Committee of the Washington University in St. Louis School of Medicine (protocol 20130156, analysis of mycobacterial pathogenesis). Washington University is registered as a research facility with the U.S. Department of Agriculture and is fully accredited by the American Association of Accreditation of Laboratory Animal Care. The Animal Welfare Assurance documentation is on file with the Office for Protection from Research Risks of the NIH. All animals used in these experiments were subjected to no or minimal discomfort. All mice were

euthanized by CO_2 asphyxiation, which is approved by the American Veterinary Medical Association Panel on Euthanasia.

Protein preparation for biochemical assays. Recombinant *Mycobacterium bovis* core RNAP was purified from *E. coli* using a system kindly supplied by Robert Landick (17, 18) as previously described (7). Recombinant *M. bovis* σ^A, which is identical to *M. tuberculosis* σ^A, was purified from *E. coli* and added to the core RNAP to reconstitute the RNAP holoenzyme.

Preparation of fluorescent promoter DNA fragments. The DNA template contains nucleotides 1470151 to 1470300 of the *M. tuberculosis* Erdman genomic DNA, which includes the *rrnA*P3 promoter. Cy3-labeled promoter DNA was prepared as previously described (8).

Stopped-flow fluorescence assay. Stopped-flow fluorescence experiments were performed as previously described (8). All experiments were performed using a final *M. bovis* RNAP-σ^A holoenzyme concentration of 225 nM and a final promoter DNA concentration of 10 nM. Experiments were performed at 25°C under the following final solution conditions: 14 mM Tris (pH 8.0), 120 mM NaCl, 10 mM $MgCl_2$, 1 mM dithiothreitol (DTT), 0.1 mg/ml BSA, and 10% glycerol by volume. Equal volume mixing of protein with promoter DNA was performed in a stopped-flow apparatus (Applied Photophysics SX-20, total shot volume 150 μl, dead time $<$ 2 ms), so the initial protein and DNA solutions were each diluted by half in order to reach their final reaction concentrations. Due to slight hardware variations in different stopped-flow instruments, excitation light was provided by either a 510 nm fixed-wavelength LED light source or a 515-nm light source from an arc lamp passed through a monochromator. The difference in excitation light had no effect on the data. In all cases emission was collected at 570+ nm using a long-pass filter. The fluorescence was monitored for 20 min.

At least two traces were collected and averaged per condition. Traces were plotted as fold change over DNA according to the formula $(F - F_0)/F_0$, where F_0 is the buffer-subtracted signal for DNA alone, and F is the buffer-subtracted signal for DNA mixed with protein. The final point of each trace was used as a measure of equilibrium fluorescence. The fold change traces were fit to a triple exponential from 0.1 to 1200 s using the ProData Viewer software from Applied Photophysics. The slowest observed rate dominated the fractional amplitude of the fits and was used as a measurement of k_{obs}^3. Conditions that were repeated multiple times on different days were used to estimate standard errors of the mean (SEM). An average SEM was used to estimate uncertainty for specific conditions that were only repeated multiple times on the same day.

***In vitro* transcription assays.** CarD proteins used in *in vitro* transcription assays were diluted into 1× dialysis buffer (20 mM Tris [pH 8.0], 150 mM NaCl, 1 mM 2-mercaptoethanol). For the aborted 3-nucleotide (nt) transcript assay (10), a linear fragment of dsDNA *M. tuberculosis* Erdman strain genomic DNA containing nucleotides 1470151 to 1470300, which includes the *M. tuberculosis rrnA*P3 promoter, was prepared by annealing and extending primers overlapping 85-bp primers (Integrated DNA Technologies, Coralville, IA). Reaction conditions were as follows: 200 nM *M. bovis* core RNAP, 2 μM *M. bovis* σ^A, 2 μM CarD or equivalent volume of buffer, 10 nM linear DNA template, 210 μM GpU dinucleotide, 21 μM UTP, 0.1 μl [α^{32}-P]UTP, 13.25 mM Tris (pH 8.0), 59 mM NaCl, 10.12 mM $MgCl_2$, 5% (vol/vol) glycerol, 1 mM DTT, and 0.1 mg/ml BSA (NEB) in a total volume of 20 μl. *M. bovis* core and σ^A were incubated for 10 min at 37°C, followed by the addition of CarD and 10 more minutes of incubation at 37°C. The DNA template was added, and the reactions were diluted to 17.5 μl, followed by incubation at 37°C for 10 min. Reaction mixtures were initiated with addition of a 2.5 μl of mixture containing GpU, UTP, and the radiolabeled UTP, followed by incubation at 37°C. After 20 min, the reactions were stopped with 2× formamide buffer (98% [vol/vol] formamide, 5 mM EDTA) and run on a 22% urea-PAGE gel. Transcripts were quantified using phosphorimaging and analyzed using Image Gauge software (FujiFilm).

ACKNOWLEDGMENTS

We thank Tim Lohman for the use of his stopped-flow spectrophotometer, Tom Ellenberger for the use of the high-pressure and fast-performance liquid chromatography in his laboratory, and Yocheved Gensler for assistance with cloning. We are grateful to Katherine Mann and Jerome Prusa for their thoughtful review of the manuscript.

We declare that we have no conflicts of interest with the contents of this article.

C.L.S. and E.A.G. are supported by grant GM107544 from the National Institutes of Health. B.E.N. is supported by grant GM118059 from the National Institutes of Health. E.A.C. is supported by grant GM114450 from the National Institutes of Health. A.L.G. is supported by the NIGMS Cell and Molecular Biology Training grant GM007067 and the Stephen I. Morse Graduate Fellowship. J.R. is supported by a Sigma-Aldrich Predoctoral Fellowship. J.P.H. is supported by National Science Foundation Graduate Research Fellowship DGE-1143954.

A.L.G., B.E.N., E.A.C., S.A.D., and C.L.S. conceived the project, designed experiments, analyzed results, and wrote the manuscript. A.L.G., J.R., J.P.H., L.A.W., L.M.O., B.B., J.C., D.J., and A.R.M. performed experiments and analyzed the results. E.A.G. analyzed results and edited the manuscript.

REFERENCES

1. WHO. 2015. Global tuberculosis report. World Health Organization, Geneva, Switzerland. http://www.who.int/tb/publications/global_report/en/.
2. Stallings CL, Stephanou NC, Chu L, Hochschild A, Nickels BE, Glickman MS. 2009. CarD is an essential regulator of rRNA transcription required for *Mycobacterium tuberculosis* persistence. Cell 138:146–159. https://doi.org/10.1016/j.cell.2009.04.041.
3. Bae B, Chen J, Davis E, Leon K, Darst SA, Campbell EA. 2015. CarD uses a minor groove wedge mechanism to stabilize the RNA polymerase open promoter complex. eLife 4:1–19.
4. Srivastava DB, Leon K, Osmundson J, Garner AL, Weiss LA, Westblade LF, Glickman MS, Landick R, Darst SA, Stallings CL, Campbell EA. 2013. Structure and function of CarD, an essential mycobacterial transcription factor. Proc Natl Acad Sci U S A 110:12619–12624. https://doi.org/10.1073/pnas.1308270110.
5. García-Moreno D, Abellón-Ruiz J, García-Heras F, Murillo FJ, Padmanabhan S, Elías-Arnanz M. 2010. CdnL, a member of the large CarD-like family of bacterial proteins, is vital for *Myxococcus xanthus* and differs functionally from the global transcriptional regulator CarD. Nucleic Acids Res 38:4586–4598. https://doi.org/10.1093/nar/gkq214.
6. Weiss LA, Harrison PG, Nickels BE, Glickman MS, Campbell EA, Darst SA, Stallings CL. 2012. Interaction of CarD with RNA polymerase mediates *Mycobacterium tuberculosis* viability, rifampin resistance, and pathogenesis. J Bacteriol 194:5621–5631. https://doi.org/10.1128/JB.00879-12.
7. Garner AL, Weiss LA, Manzano AR, Galburt EA, Stallings CL. 2014. CarD integrates three functional modules to promote efficient transcription, antibiotic tolerance, and pathogenesis in mycobacteria. Mol Microbiol 93:682–697. https://doi.org/10.1111/mmi.12681.
8. Rammohan J, Ruiz Manzano A, Garner AL, Stallings CL, Galburt EA. 2015. CarD stabilizes mycobacterial open complexes via a two-tiered kinetic mechanism. Nucleic Acids Res 43:3272–3285. https://doi.org/10.1093/nar/gkv078.
9. Gulten G, Sacchettini JC. 2013. Structure of the *M. tuberculosis* CarD/RNAP β-lobes complex reveals the molecular basis of interaction and presents a distinct DNA-binding domain for *M. tuberculosis* CarD. Structure 21:1859–1869. https://doi.org/10.1016/j.str.2013.08.014.
10. Davis E, Chen J, Leon K, Darst SA, Campbell EA. 2015. Mycobacterial RNA polymerase forms unstable open promoter complexes that are stabilized by CarD. Nucleic Acids Res 43:433–445. https://doi.org/10.1093/nar/gku1231.
11. Raju RM, Unnikrishnan M, Rubin DHF, Krishnamoorthy V, Kandror O, Akopian TN, Goldberg AL, Rubin EJ. 2012. *Mycobacterium tuberculosis* ClpP1 and ClpP2 function together in protein degradation and are required for viability in vitro and during infection. PLoS Pathog 8:e1002511. https://doi.org/10.1371/journal.ppat.1002511.
12. Bremer H, Dennis PP. 1996. Modulation of chemical composition and other parameters of the cell by growth rate, p 1553–1569. *In Escherichia coli* and *Salmonella* Typhimurium: cellular and molecular biology. ASM Press, Washington, DC.
13. Schaechter M, Maaloe O, Kjeldgaard NO. 1958. Dependency on medium and temperature of cell size and chemical composition during balanced growth of *Salmonella typhimurium*. J Gen Microbiol 19:592–606. https://doi.org/10.1099/00221287-19-3-592.
14. Binder BJ, Liu YC. 1998. Growth rate regulation of rRNA content of a marine *Synechococcus* (cyanobacterium) strain. Appl Environ Microbiol 64:3346–3351.
15. Nickels BE. 2009. Genetic assays to define and characterize protein-protein interactions involved in gene regulation. Methods 47:53–62. https://doi.org/10.1016/j.ymeth.2008.10.011.
16. Pashley CA, Parish T. 2003. Efficient switching of mycobacteriophage L5-based integrating plasmids in *Mycobacterium tuberculosis*. FEMS Microbiol Lett 229:211–215. https://doi.org/10.1016/S0378-1097(03)00823-1.
17. Huff J, Czyz A, Landick R, Niederweis M. 2010. Taking phage integration to the next level as a genetic tool for mycobacteria. Gene 468:8–19. https://doi.org/10.1016/j.gene.2010.07.012.
18. Czyz A, Mooney RA, Iaconi A, Landick R. 2014. Mycobacterial RNA polymerase requires a U-tract at intrinsic terminators and is aided by NusG at suboptimal terminators. mBio 5:1–10. https://doi.org/10.3391/mbi.2014.5.1.01.